

A METHOD FOR QUANTIFYING THE IMPACTS AND
INTERACTIONS OF POTENTIAL-VORTICITY
ANOMALIES IN EXTRATROPICAL CYCLONES:
MEDITERRANEAN EXAMPLE

R. Romero

Grup de Meteorologia, Departament de Física, Universitat de les Illes Balears, Palma de Mallorca, Spain

Contribution to “XVII Jornades de Meteorologia Eduard Fontseré”

1. Introduction

Since the seminal paper of Hoskins et al. (1985), the use of potential vorticity to analyse the genesis and evolution of synoptic-scale systems has become very popular in Meteorology. The two powerful principles of conservation and invertibility can be readily combined to develop a conceptually elegant framework that extends the capabilities of the more traditional quasigeostrophic theory for explaining the dynamics of mid-latitude circulation systems. This method of dynamical analysis has been referred to as “PV thinking”.

Extratropical cyclogenesis is the best paradigm of cooperation between anomalies of different origin to reinforce each other. The vertical interaction between the upper-level wavelike PV anomaly and the potential temperature field along the lower boundary is fundamental to explain the baroclinic growth of the disturbance (Hoskins et al. 1985): as the upper-level cyclonic PV anomaly arrives over a region of significant low-level baroclinicity, its induced circulation will promote warm advection east of it, creating a warm anomaly at surface, which in turn will induce its own cyclonic circulation that is felt just to the east of the upper-level positive PV anomaly, thus contributing to its amplification by the southward advection of the high PV values found at higher latitudes, a positive feedback mechanism that will be reflected as the growth of the wave-cyclone system in this idealized dry atmosphere. For the real, moist atmosphere, the generation of low-level PV anomalies is due not only to advection but also to differential surface heating and condensation of water vapor in the atmospheric column. The role of latent heat release for accelerating the growth of the disturbance is well recognized, and this factor has been included explicitly in the PV framework by some authors (e.g. Davis and Emanuel 1991).

In this work I present a “dynamic” approach that allows us to isolate quantitatively the previous impacts and interactions of the PV anomalies during the life cycle of the cyclone. The method utilizes the factor separation technique (Stein and Alpert 1993), applied to the prognostic system of balance equations associated with the piecewise PV inversion technique described in Davis and Emanuel (1991). The potentialities of this method will be illustrated for the 10-12 November 2001 western Mediterranean cyclone, the worst storm affecting the Balearic Islands during the last decades (further details can be found in Romero 2008).

2. The Mediterranean cyclone of 10-12 November 2001

This extraordinary cyclone originated over the north African lands over a region of marked baroclinicity, preceded by a significant cold air intrusion at upper levels from north-central Europe towards Iberia and Morocco. During this incipient phase on 9-10 November, catastrophic flash floods occurred in Algeria and Morocco. As the cyclone evolved northeastwards into the western Mediterranean basin the central pressure continued to deepen and an appreciable pressure gradient developed around its core, leading to the mature or most intense state of the cyclone at around 11 November 00 UTC (Fig. 1a). At this time the warm and cold fronts signatures in the low-level thermal field are both very clear and occlusion is suggested near the tip of the warm air surge from north Africa induced by the circulation (same figure). Meanwhile, the upper-level circulation adopted cut-off characteristics and two geopotential height minima are visible, located to the west and east of Gibraltar Strait at 11 November 00 UTC (Fig. 2b). Most of the rainfall and the main wind-induced damage in the Balearic Islands (located in the centre of the western Mediterranean) occurred during this mature phase of the cyclone. The period 11-12 November corresponds to the decay of the disturbance: the low pressure system filled as it progressed further northwards and the thermal gradient weakened appreciably. Interestingly, the two upper-level embedded disturbances rotated cyclonically about each other as the large scale parent trough entered the western Mediterranean.

Although the primary role of baroclinic instability is quite clear, the high precipitation potential of this cyclone and the massive cloudy structures that could be observed during the oceanic phase of the storm suggest that condensational latent heat release could have also played a role for the cyclone development. Therefore, diabatically generated PV within the cloud systems will be considered as an explicit factor in the subsequent analysis.

We will consider a simple but physically meaningful decomposition of the perturbation PV field q' , which is appropriate to interpret the baroclinic event according to the processes emphasized by the PV thinking theory. The perturbation PV field is defined every 12 h (at 00 and 12 UTC, the available analysis times) during the life cycle of the storm, as the departure from the seven-day time average for the period from 00 UTC on 7 November to 00 UTC on 14 November. We will refer to such reference state as the *MEAN* flow. Three unique anomalies are defined (see Table 1): *ULev* is associated with the undulating tropopause and will contain the PV perturbation above 700 hPa plus

the potential temperature perturbation θ' field at the upper boundary, located at 100 hPa; $LLev$ represents the surface baroclinicity since it is composed of θ' at the bottom boundary (1000 hPa) and the lower-level interior PV perturbation, up to 700 hPa; $DIAB$ is expressed as the positive PV perturbation below 500 hPa in areas with greater than 70% relative humidity. The latter is defined to account for the lower-tropospheric PV anomalies associated with condensational heating. Wherever the interior q' is assigned to $DIAB$ according to the previous definition, it will be removed from $ULev$ or $LLev$. Thus we can refer unambiguously to $ULev$ and $LLev$ as the dry PV anomalies, associated with the baroclinic processes, and to $DIAB$ as a moist anomaly, related with the diabatic contribution of clouds and precipitation. It is important to note that at any point of the interior domain the sum of $ULev$, $LLev$ and $DIAB$ equals the total perturbation field q' , as well as the total θ' field at the boundaries. These anomalies, together with the $MEAN$ state, define the total q and θ fields. Note also that $ULev$ and $LLev$ incorporate both positive and negative PV anomalies (e.g. upper-level troughs and ridges and warm and cold surface anomalies, respectively), whereas $DIAB$ is positive everywhere.

The patterns of $ULev$, $LLev$ and $DIAB$ at the mature phase of the storm are depicted in Fig. 2a for some specific isobaric levels. Relevant signatures emphasized previously, such as the two upper-level embedded disturbances, the marked low-level baroclinicity, and the massive cloud formation over the western Mediterranean, are well identified on this PV chart. The inverted balance fields from these anomalies after applying the piecewise PV inversion technique of Davis and Emanuel (1991) are presented in Fig. 2b. Both height deficits (i.e. cyclonic vorticity) and height increases (anticyclonic vorticity) can be found in connection with the dry PV anomalies owing to its double signed pattern; perturbations of both signs alternate across the whole domain following the synoptic wave train structure. Since the moist $DIAB$ anomaly is positive definite it only produces negative height perturbations, essentially in the form of a localized cyclonic vortex over the area of influence of the cyclone. A significant negative height contribution results from each PV anomaly over the area of the surface cyclone (letter C in 2b), thus cooperating with each other to explain the intense barometric depression.

The above PV-inversion results provide a merely static depiction of the cyclogenesis/cyclolysis process, in the sense that only the contributions to the instantaneous cyclone intensity by the selected PV anomalies can be quantitatively diagnosed. Within the framework of PV-thinking theory, it would

be illuminating to isolate with similar degree of detail the true impact of the PV anomalies on the cyclone behaviour (i.e. on changes in its growth, decay, size, trajectory or shape), by means, for example, of the induced surface pressure tendency and vertical motion. More importantly, it would be quite useful to split the contribution of each PV anomaly among its individual effect and the effects produced by its interaction with the other PV features or the mean flow. We could refer to this new perspective as a dynamic approach of the PV-based diagnosis of cyclones. The following method develops such idea.

3. PV-based prognostic system combined with the factor separation method

A set of prognostic balance equations can be derived from the PV diagnostic system presented in Davis and Emanuel (1991). We start by obtaining equations for geopotential and streamfunction tendencies (ϕ^t, ψ^t) by taking the local time derivatives of Charney (1955) nonlinear balance equation and the approximate form of Ertel's PV (Rossby 1940; Ertel 1942):

$$\nabla^2 \phi^t = \nabla \cdot f \nabla \psi^t + 2m^2 \left[\frac{\partial^2 \psi^t}{\partial x^2} \frac{\partial^2 \psi}{\partial y^2} + \frac{\partial^2 \psi}{\partial x^2} \frac{\partial^2 \psi^t}{\partial y^2} - 2 \frac{\partial^2 \psi}{\partial x \partial y} \frac{\partial^2 \psi^t}{\partial x \partial y} \right] \quad (1)$$

$$q^t = \frac{g\kappa\pi}{p} \left[(f + m^2 \nabla^2 \psi) \frac{\partial^2 \phi^t}{\partial \pi^2} + m^2 \frac{\partial^2 \phi}{\partial \pi^2} \nabla^2 \psi^t - m^2 \left(\frac{\partial^2 \psi^t}{\partial x \partial \pi} \frac{\partial^2 \phi}{\partial x \partial \pi} + \frac{\partial^2 \psi}{\partial x \partial \pi} \frac{\partial^2 \phi^t}{\partial x \partial \pi} + \frac{\partial^2 \psi^t}{\partial y \partial \pi} \frac{\partial^2 \phi}{\partial y \partial \pi} + \frac{\partial^2 \psi}{\partial y \partial \pi} \frac{\partial^2 \phi^t}{\partial y \partial \pi} \right) \right] \quad (2)$$

where f is the Coriolis parameter, m denotes the map-scale factor of the particular projection used, p is the pressure, g the gravity, $\kappa = R_d/C_p$ and the vertical coordinate π is the Exner function $C_p(p/p_0)^\kappa$.

Recalling that ϕ (geopotential) and ψ (streamfunction) are known aspects of the circulation after the inversion of q in last section, the system (1)-(2) can be solved for the geopotential and streamfunction tendencies provided q^t is known. This can be calculated using the following form of Ertel's PV tendency equation:

$$q^t = -m(\mathbf{V}_\psi + \mathbf{V}_\chi) \cdot \nabla q - \omega^* \frac{\partial q}{\partial \pi} + \frac{m}{\rho} \boldsymbol{\eta} \cdot \nabla LH, \quad (3)$$

where the vertical velocity $\omega^* \equiv d\pi/dt$ and irrotational wind \mathbf{V}_χ must be formally retained (Krishnamurti 1968; Iversen and Nordeng 1984), meaning that we cannot simply advect q with the

nondivergent wind \mathbf{V}_ψ . The horizontal winds are given by the familiar expressions $\mathbf{V}_\psi = m\mathbf{k} \times \nabla\psi$ and $\mathbf{V}_\chi = m\nabla\chi$, and ω^* is related with the more traditional vertical velocity in pressure coordinates (ω) through the expression $\omega^* = (\kappa\pi/p)\omega$. In addition, the only nonconservative effect that is included in this equation is the latent heat release $LH \equiv d\theta/dt$ from nonconvective clouds where the air is ascending on a broad scale. This diabatic term is parameterized in terms of ω^* as explained in Davis and Emanuel (1991).

The prognostic system is closed by means of an omega equation for ω^* and the continuity equation for the velocity potential χ , which in this context take the following forms:

$$\begin{aligned}
& f\eta \frac{\partial}{\partial\pi} \left[\pi^{1-1/\kappa} \frac{\partial}{\partial\pi} (\pi^{1/\kappa-1} \omega^*) \right] + m^2 \nabla^2 \left(\frac{\partial^2 \phi}{\partial\pi^2} \omega^* \right) \\
& - m^2 f \frac{\partial}{\partial\pi} \left(\frac{\partial\omega^*}{\partial x} \frac{\partial\psi}{\partial x \partial\pi} + \frac{\partial\omega^*}{\partial y} \frac{\partial\psi}{\partial y \partial\pi} \right) \\
& + \left(f \frac{\partial\eta}{\partial\pi} \frac{1/\kappa - 1}{\pi} - f \frac{\partial^2 \eta}{\partial\pi^2} \right) \omega^* = m^3 \nabla^2 [(\mathbf{V}_\psi + \mathbf{V}_\chi) \cdot \nabla\theta] \\
& + mf \frac{\partial}{\partial\pi} [(\mathbf{V}_\psi + \mathbf{V}_\chi) \cdot \nabla\eta] - m^2 \nabla f \cdot \nabla \left(\frac{\partial\psi^t}{\partial\pi} \right) \\
& - 2m^4 \frac{\partial}{\partial\pi} \left[\frac{\partial^2 \psi^t}{\partial x^2} \frac{\partial^2 \psi}{\partial y^2} + \frac{\partial^2 \psi}{\partial x^2} \frac{\partial^2 \psi^t}{\partial y^2} - 2 \frac{\partial^2 \psi}{\partial x \partial y} \frac{\partial^2 \psi^t}{\partial x \partial y} \right] \\
& - m^2 \nabla^2 LH
\end{aligned} \tag{4}$$

$$m^2 \nabla^2 \chi + \pi^{1-1/\kappa} \frac{\partial}{\partial\pi} (\pi^{1/\kappa-1} \omega^*) = 0 \tag{5}$$

The complete system of equations (1)-(5), formulated in finite differences with vertical staggering of the ω^* levels, is solved iteratively by a simultaneous relaxation method for the fields ϕ^t , ψ^t , q^t , ω^* and χ . It is important to note that the equations are not integrated in time, but simply solved for the instantaneous tendencies. Homogeneous lateral boundary conditions are applied on a large enough domain for each field (i.e. $\phi^t = \psi^t = q^t = \omega^* = \chi = 0$), whereas at the top and bottom boundaries more complex conditions are used: the vertical velocity is zero and topographic, respectively; and Neumann type definitions are used for the tendencies ϕ^t and ψ^t :

$$\partial\phi^t/\partial\pi = f\partial\psi^t/\partial\pi = -\theta^t \tag{6}$$

where the necessary potential temperature tendencies at both levels are evaluated from the thermodynamic equation:

$$\theta^t = -m(\mathbf{V}_\psi + \mathbf{V}_\chi) \cdot \nabla\theta - \omega^* \frac{\partial\theta}{\partial\pi} + LH \quad (7)$$

The prognostic system is solved at 00 and 12 UTC during the life cycle of the Mediterranean cyclone. Of particular interest for describing the cyclogenesis process is the calculated field of surface height tendency around the storm. This field is plotted as unshaded line contours in Fig. 3 for 11 November 00 UTC (storm's peak intensity time). As expected, the obtained result identifies the strong cyclogenesis that took place over the western Mediterranean basin at that time (recall Fig. 1). Since this result emerges from the total balance flow, described by q , ϕ and ψ , we could refer to its signature in Fig. 3 as the **total** field for the surface height tendency.

In the present context we are searching a way to split the total field into the **contributions** by the four constituent PV elements of q (i.e. the basic state *MEAN* plus the three anomalies *ULev*, *LLev* and *DIAB*), including all their possible lateral and vertical interactions. This appears to be a feasible task based on our ability of repeating the above calculations after subtracting from the input (q, ϕ, ψ) flow state one or several PV anomalies and their associated flows. This is, in essence, a factor separation exercise as presented in Stein and Alpert (1993). With three factors, 8 distinct flow configurations are necessary (see Table 2). The complete set of effects can be isolated through the algebraic combination of the corresponding solutions:

- $E_0 = F_0$
- $E_1 = F_1 - F_0$
- $E_2 = F_2 - F_0$
- $E_3 = F_3 - F_0$
- $E_{12} = F_{12} - (F_1 + F_2) + F_0$
- $E_{13} = F_{13} - (F_1 + F_3) + F_0$
- $E_{23} = F_{23} - (F_2 + F_3) + F_0$
- $E_{123} = F_{123} - (F_{12} + F_{13} + F_{23}) + (F_1 + F_2 + F_3) - F_0$

In the following, a more intuitive notation is adopted for these effects by using the terms *MEAN*, *ULev*, *LLev*, *DIAB*, *ULev/LLev*, *ULev/DIAB*, *LLev/DIAB* and *ULev/LLev/DIAB*, respectively.

4. PV thinking in action: Results of the dynamic approach

The impacts and interactions of the potential vorticity anomalies on the surface height tendency are plotted for the mature storm in Fig. 3, as spatial patterns with positive and negative signals of the eight different contributions to the total field (this is also included in the figure for reference). Particular attention is paid to signatures of negative height tendency occurring over the western Mediterranean region, thus contributing to the cyclogenesis mechanism.

The action of the background flow *MEAN* is to help propagate the surface cyclone eastwards along the Mediterranean waters (Fig. 3a). The individual effect of *ULev* is crucial for the cyclogenesis (Fig. 3b). It is responsible for a significant fraction of the surface pressure fall calculated over the western Mediterranean.

Individually, *LLev* represents also a significant contribution to the cyclone growth, movement and decay. During the mature phase its main action is concentrated along the northern flank of the cyclone (Fig. 3c), that is, in the zones affected by well defined surface fronts and where the warm advection is most clear. Thus the pattern of the *LLev* contribution favours the northeastward propagation of the surface disturbance that was emphasized in section 2.

The very localized nature of the *DIAB* PV anomaly (Fig. 2a) implies a comparatively weak individual effect on the surface height tendency (Fig. 3d). This effect is essentially linked to the PV advection induced by the background flow and therefore adopts a dipolar structure about the Algerian coast surrounding the anomaly.

The *ULev/LLev* interaction is a leading agent for generating and driving the November 2001 cyclone (Fig. 3e), in agreement with the conceptual model of baroclinic developments formulated by the PV thinking theory. On the surface height tendency this factor attains a comparable or even higher magnitude than the abovementioned individual contribution of *ULev* (compare with Fig. 3b), with the particularity that the pattern over the western Mediterranean resembles very much the total tendency field. The importance of the synergistic action is well understood taking in mind the appreciable warm advection values that are induced at low levels.

The $ULev/DIAB$ effect is quite relevant (Fig. 3f). It displays a dipolar structure as the one noted for $DIAB$ (Fig. 3d), except of larger magnitude and reversed sign. The sign reversal is due to the opposite directions of the $MEAN$ and $ULev$ advective winds acting, respectively, on the $DIAB$ PV anomaly (not shown). With all, the $ULev/DIAB$ factor is contributing to cyclogenesis only to the west of the cyclone; over the cyclone position and eastwards, its effect is essentially cyclolytic (Fig. 3f).

The $LLev/DIAB$ synergism is also cyclolytic over the mature cyclone (Fig. 3g). Since the $LLev/DIAB$ mechanism incorporates the effects of the $DIAB$ PV advection by the $LLev$ -induced flow and the $LLev$ thermal advection by the $DIAB$ -induced flow, both of comparable magnitude, the precise interpretation of the $LLev/DIAB$ spatial pattern displayed on Fig. 3g appears to be more intricate than for the other factors.

Finally, we can analyse the contribution of the triple interaction $ULev/LLev/DIAB$ (Fig. 3h). Owing to the involvement of the small $DIAB$ PV anomaly in this factor, it exerts only a secondary role, like $DIAB$, $ULev/DIAB$ and $LLev/DIAB$. Interestingly, the obtained height tendency pattern almost perfectly balances with the $LLev/DIAB$ contribution (compare with Fig. 3g), helping in this case to the deepening of the cyclone.

5. Conclusion

In summary, it can be concluded¹ that the most intense phase of the November 2001 Mediterranean cyclone was regulated by the $MEAN$, $ULev$, $LLev$ and $ULev/LLev$ processes: $MEAN$ and $LLev$ assisted in the northeastward propagation of the disturbance and to some extent to its intensification, especially $LLev$ during its African phase; both $ULev$ and $ULev/LLev$ were fundamental for the African cyclogenesis and further intensification of the disturbance over the western Mediterranean, although $ULev/LLev$ quickly decayed after the cyclone maturation. The remaining mechanisms ($DIAB$, $ULev/DIAB$, $LLev/DIAB$ and $ULev/LLev/DIAB$) were most relevant during the mature phase of the system but, compared to the first group, they only exerted a secondary role owing to the limited strength and spatial dimensions of the $DIAB$ PV anomaly. According to the factor separation results, the development and mature phases of the baroclinic disturbance can be described as a meteorological scenario of effective cooperation among the background flow and

¹For a deeper discussion, which includes also results for the development and decay phases of the baroclinic system, see Romero (2008).

the PV anomalies over the surface cyclone domain, whereas the decay of the system is linked to a scenario of much weaker or even cyclolytic interactions between some of these factors.

REFERENCES

- Charney, J. G., 1955: The use of primitive equations of motion in numerical prediction. *Tellus*, **7**, 22-26.
- Davis, C. A. and Emanuel, K. A., 1991: Potential vorticity diagnostics of cyclogenesis. *Mon. Wea. Rev.*, **119**, 1929-1953.
- Ertel, H., 1942: Ein neuer hydrodynamischer wirbelsatz. *Meteor. Z.*, **59**, 271-281.
- Hoskins, B. J, McIntyre, M. E. and Robertson, A. W., 1985: On the use and significance of isentropic potential vorticity maps. *Quart. J. Roy. Meteor. Soc.*, **111**, 877-946.
- Iversen, T., T. E. Nordeng, 1984: A hierarchy of nonlinear filtered models-numerical solutions. *Mon. Wea. Rev.*, **112**, 2048-2059.
- Krishnamurti, T. N., 1968: A diagnostic balanced model for studies of weather systems of low and high latitudes, Rossby number less than 1. *Mon. Wea. Rev.*, **96**, 197-207.
- Romero, R., 2008: A method for quantifying the impacts and interactions of potential-vorticity anomalies in extratropical cyclones. *Quart. J. R. Meteorol. Soc.*, **134**, 385-402.
- Rossby, C. G., 1940: Planetary flow patterns in the atmosphere. *Quart. J. Roy. Meteor. Soc.*, **66**, (Suppl) 68-87.
- Stein, U. and Alpert, P., 1993: Factor separation in numerical simulations. *J. Atm. Sci.*, **50**, 2107-2115.

TABLES

PV anomaly	Definition
<i>ULev</i>	PV perturbation above 700 hPa
<i>LLev</i>	Surface thermal anomaly and PV perturbation below 700 hPa
<i>DIAB</i>	Positive PV perturbation below 500 hPa in areas with relative humidity exceeding 70%

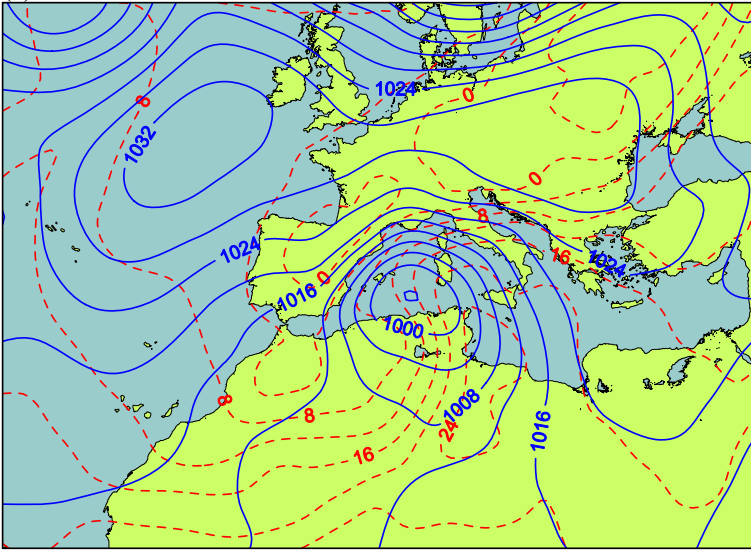
Table 1: Definition of the PV anomalies used in the study of the 10-12 November 2001 cyclone, associated with mid-upper tropospheric levels (*ULev*), low tropospheric levels (*LLev*), and condensational diabatic processes (*DIAB*).

FLOW STATE	0: MEAN	1: ULev	2: LLev	3: DIAB
F_0	Yes	No	No	No
F_1	Yes	Yes	No	No
F_2	Yes	No	Yes	No
F_3	Yes	No	No	Yes
F_{12}	Yes	Yes	Yes	No
F_{13}	Yes	Yes	No	Yes
F_{23}	Yes	No	Yes	Yes
F_{123}	Yes	Yes	Yes	Yes

Table 2: The eight different atmospheric flow states that are calculated using the PV-based prognostic system for the analysis of the 10-12 November 2001 cyclone. The results are combined in the factor separation method (see text).

(a) SLP and T925

11 Nov 00 UTC



(b) H500 and T500

11 Nov 00 UTC

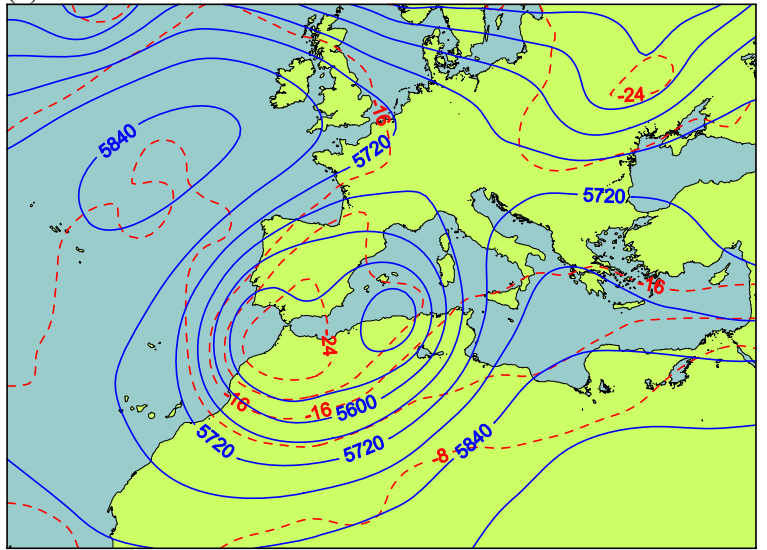


Figure 1: Synoptic situation on 11 November 2001 00 UTC. The following fields are shown: (a) Sea level pressure (blue solid line using 4 hPa contour intervals) and temperature at 925 hPa (red dashed line using 4 °C intervals); (b) Geopotential height at 500 hPa (blue solid line using 60 gpm contour intervals) and temperature at 500 hPa (red dashed line using 4 °C intervals).

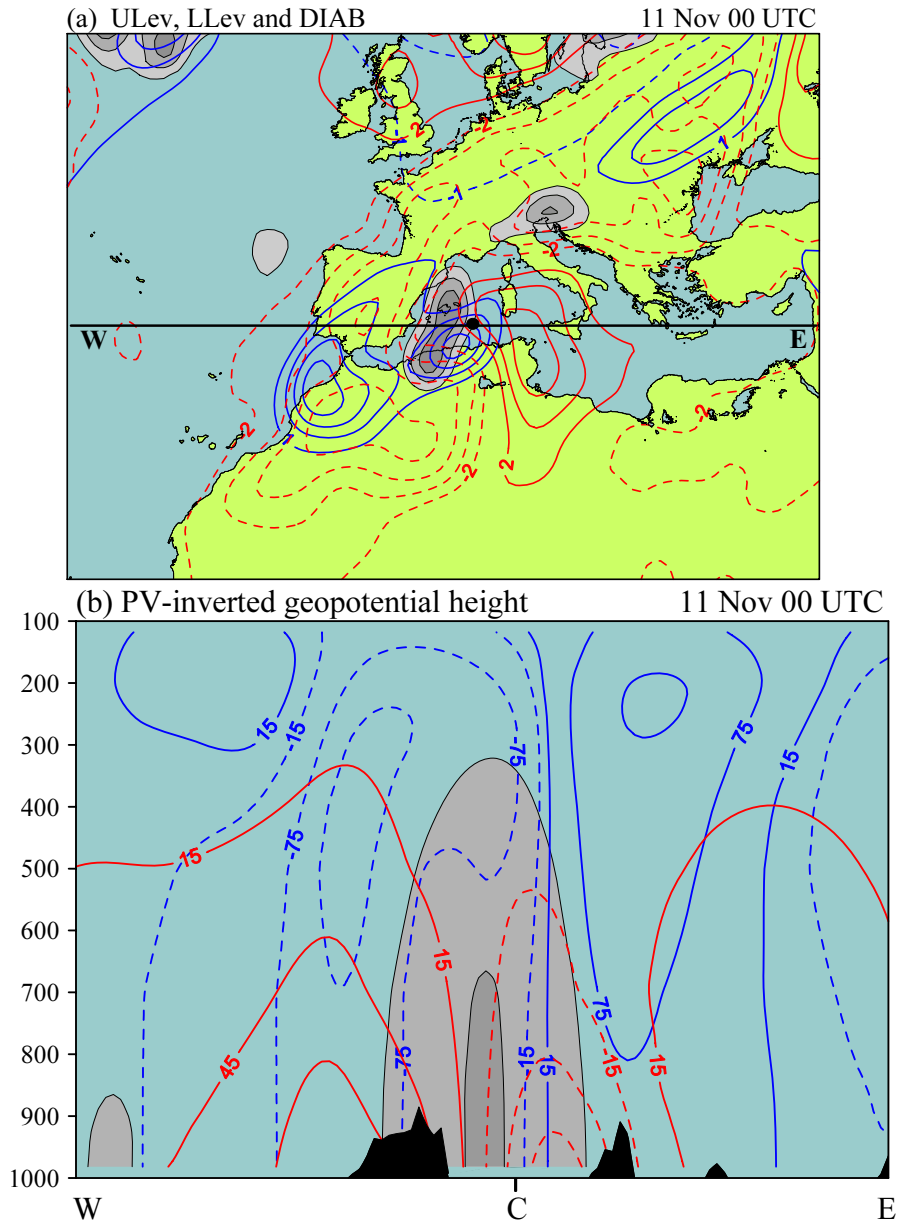


Figure 2: (a) Depiction of the PV anomalies defined in the study ($ULev$, $LLev$ and $DIAB$; see Table 1) on 11 November 00 UTC. $ULev$ is shown at 300 hPa using blue contours (solid and dashed lines indicate positive and negative values of the PV anomaly, respectively, starting at 1 and -1 PVU every 1.5 PVU); $LLev$ is depicted by means of the thermal boundary condition at 1000 hPa using red contours (solid and dashed lines indicate positive and negative values of the temperature anomaly, respectively, starting at 2 and -2 $^{\circ}\text{C}$ every 2 $^{\circ}\text{C}$); $DIAB$ is shown at 700 hPa as grey shaded contours, starting at 0.1 PVU every 0.1 PVU. (b) Vertical cross section along the line WE shown in (a) of the PV-inverted geopotential height perturbation field. Blue contours represent the field inverted from $ULev$ (positive and negative values in continuous and dashed lines, respectively, starting at 15 and -15 m every 60 m); red contours depict the field inverted from $LLev$ (positive and negative values continuous and dashed, respectively, starting at 15 and -15 m every 30 m); and grey shaded contours represent the $DIAB$ -inverted field (contours every 30 m starting at -15 m). Letter C at the bottom of the figure indicates the position of the cyclone.

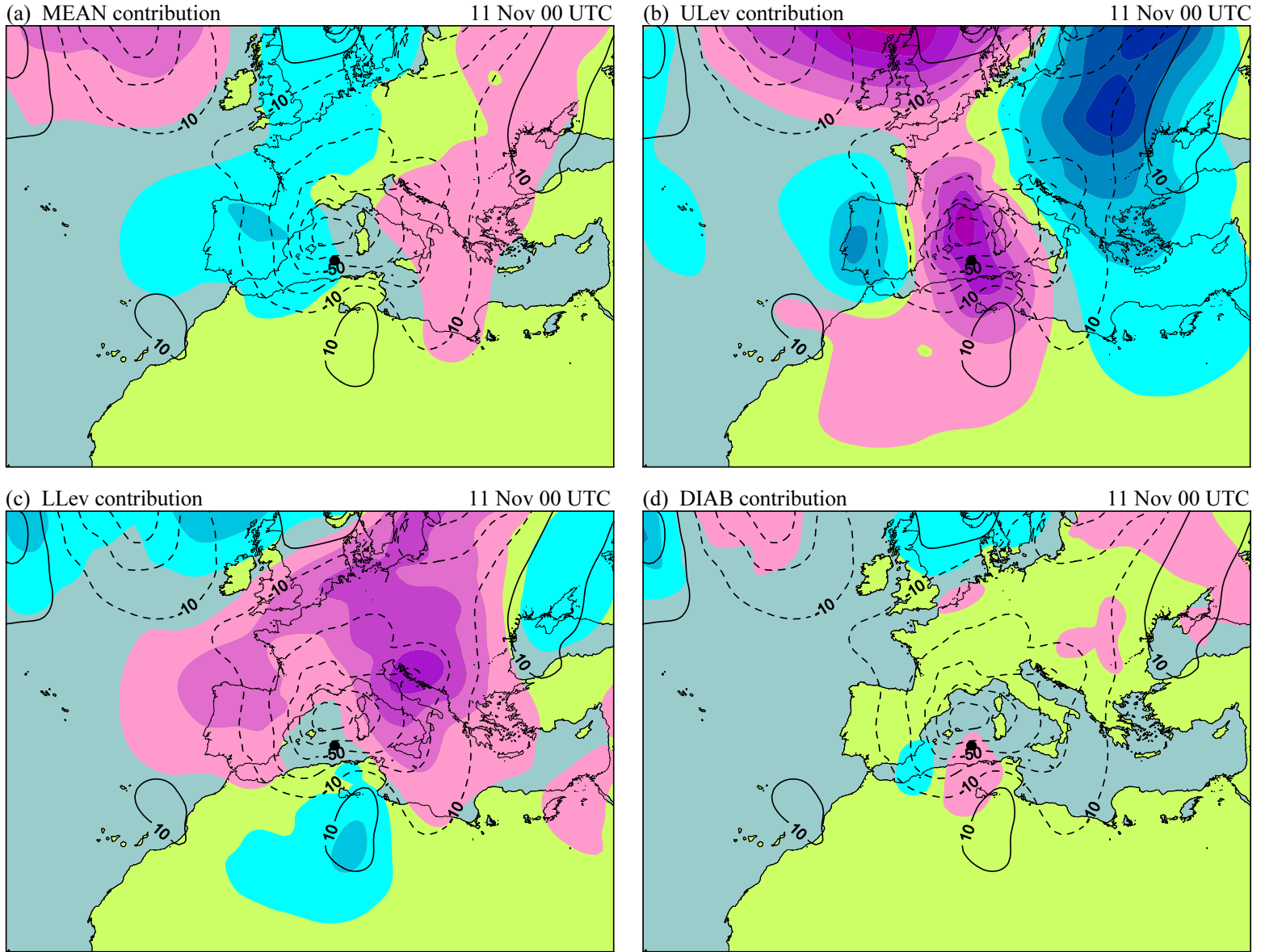
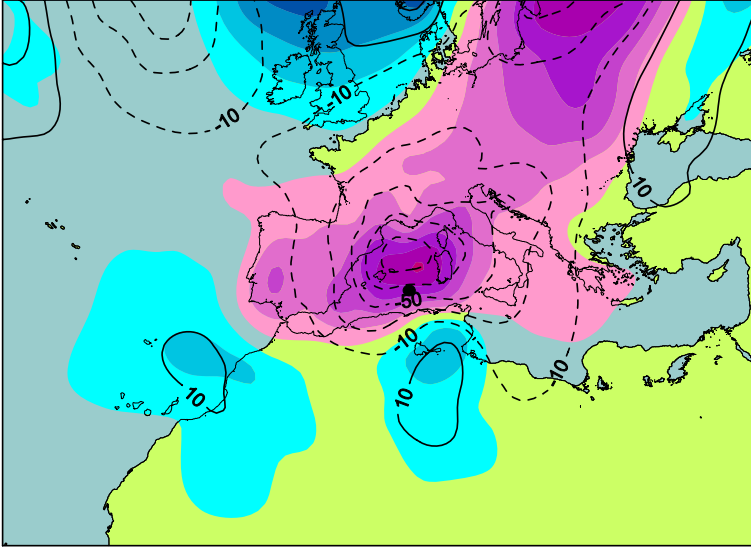
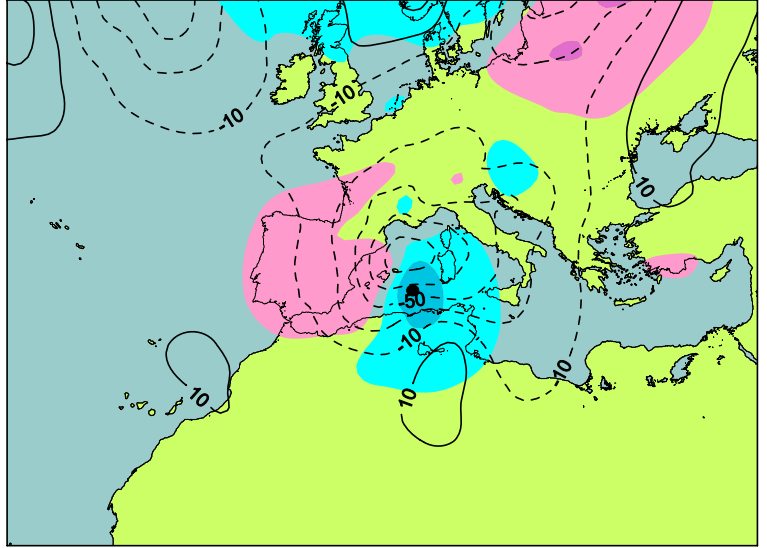


Figure 3: Factor separation results on the geopotential height tendency at 925 hPa, corresponding to the mature phase of the cyclone (11 November 00 UTC). The contributions by (a) *MEAN*, (b) *ULev*, (c) *LLev*, (d) *DIAB*, (e) *ULev/LLev*, (f) *ULev/DIAB*, (g) *LLev/DIAB* and (h) *ULev/LLev/DIAB* are shown as pink shaded regions for negative height tendency and blue shaded regions for positive height tendency, starting at -5 and +5 gpm/12 h, respectively, with a contour interval of 10 gpm/12 h. In all figures, the total height tendency field at 925 hPa is also shown, starting at -10 (dashed line) and +10 gpm/12 h (continuous line), with a contour interval of 20 gpm/12 h. The black circle depicted in the southern Mediterranean indicates the central position of the cyclone (see Fig. 1).

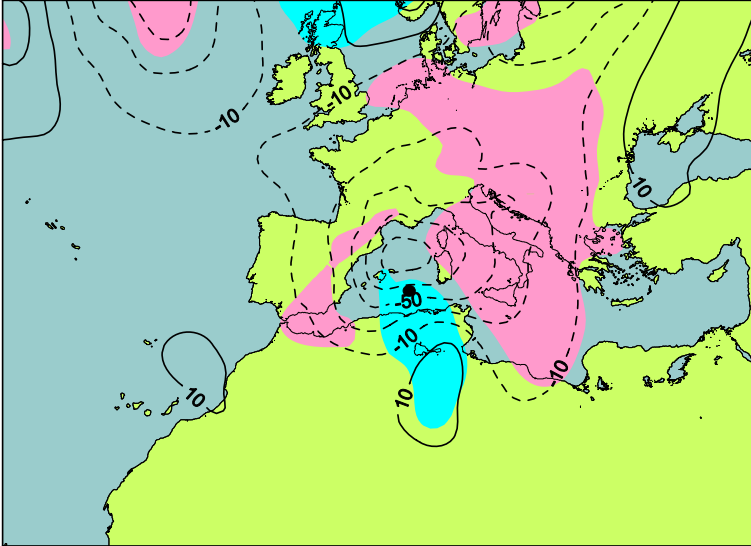
(e) ULev/LLev contribution 11 Nov 00 UTC



(f) ULev/DIAB contribution 11 Nov 00 UTC



(g) LLev/DIAB contribution 11 Nov 00 UTC



(h) ULev/LLev/DIAB contribution 11 Nov 00 UTC

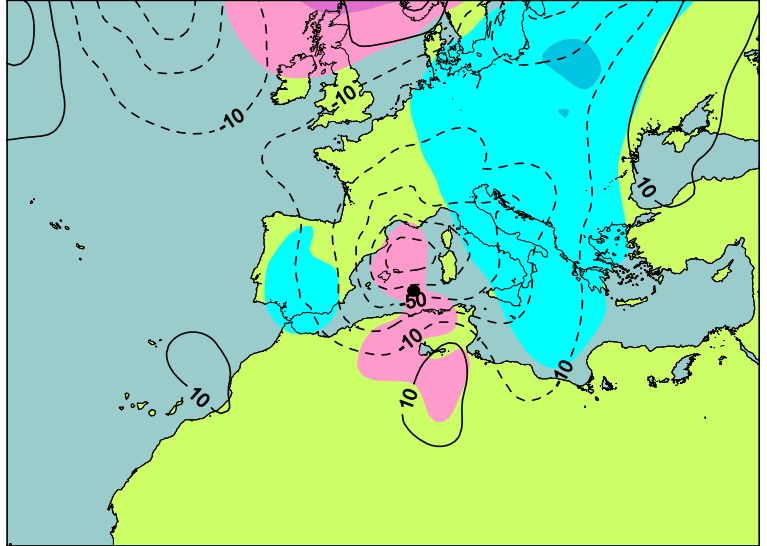


Figure 3 (continuation).